

Study of structural, morphological and optical properties of ZnO and Mg-doped ZnO thin films synthesized by evaporation technique

S. A. Hussain^a, I. A. Khan^a, M. Ayub^b, A. Rasheed^{a*}

^a*Department of Physics, Government College University Faisalabad, 38000, Faisalabad, Pakistan*

^b*Department of Physics, Mirpur University of Science and Technology, 10250, Mirpur, A.K, Pakistan*

Un-doped ZnO and Mg-doped ZnO thin films (TFs) are synthesized by evaporation technique. The synthesized un-doped ZnO TFs are exposed to evaporated Mg contents for different times. XRD patterns reveal the development of (100), (002), (101) planes related to ZnO phase. The shifting of diffraction planes and shrinking of lattice parameters confirms the doping of Mg contents into ZnO lattice. The crystallite size of (100), (101) and (002) planes lies in the range from (12.43-14.51 nm), (14.28-19.08 nm) and (14.78-19.19 nm) respectively. SEM analysis indicates that the formation of nano-fibers and nano-chains of rounded nanoparticles. EDX analysis confirms the presence of Zn, O and Mg whose amount is increased with increasing exposure time. The energy band gap (E_g) of un-doped ZnO (~ 3.05 eV) is increased to $\Sigma 3.08$, $\Sigma 3.19$ and $\Sigma 3.29$ eV) with increasing exposure time in Mg contents.

(Received July 16, 2021; Accepted December 6, 2021)

Keywords: XRD, SEM, Thermal evaporator, ZnO, Mg-ZnO, Energy band gap

1. Introduction

Zinc oxide (ZnO) is a semiconductor material having wide energy band gap (3.36 eV), high exciton binding energy (60 meV) and remarkable applications in optoelectronics devices, solar cell, liquid crystal display, photoconductors and sensors [1-7]. Most of research work has been done by researchers related to ZnO material, however, it is necessary to alter its crystal structure by doping of different elements which will change the surface properties like structural, morphological, electrical and optical. The major doping elements which may use to modify the crystal structure of ZnO are Al, Ga, Mg, Ca and Cd [8]. Noticeably, the doping is a possible approach of modifying the energy band gap of ZnO which shifts the Fermi level by creating impurity states [9]. It is necessary to consider the radius of dopant element because the dopant atoms of similar radius are recommendable to produce compound material with less lattice distortion. Mg is a suitable dopant element because its ionic radius (0.57 Å) is close to the ionic radius (0.60 Å) of Zn. Therefore, the Mg cannot only replace the Zn atoms in ZnO lattice but also incorporate interstitially creating point defects, vacancies and residual stresses which are responsible to change the film surface properties. It is well known that the energy band gap of ZnO lattice can be tuned by Mg doping [10-12]. Therefore, the Mg doped ZnO thin films (Mg-ZnO TFs) are of huge interest in many applications like light emitting diode and solar cells. The values of energy band gap of ZnO is increased from 3.3 eV to 7.5 eV by Mg doping [12-14]. Moreover, the Mg doping not only changes the structural properties but also enhance the energy band gap of ZnO, however, energy band gap of ZnO depends on dopant (Mg) contents. Interestingly, the Mg makes phase separation when its higher contents was doped in ZnO lattice [10, 15]. Therefore, it is difficult to achieve single phase hexagonal Mg-ZnO especially when Mg content is higher than optimum amount [11, 16].

Various deposition techniques like molecular beam epitaxy, metal organic chemical vapor deposition, plasma enhanced chemical deposition, R F magnetron sputtering, atomic layer

* Corresponding author: abdurrasheed@gcuf.edu.pk

deposition, pulsed laser deposition, electron beam evaporation [17, 18] are being used to synthesized ZnO and Mg-ZnO TFs. These synthesis technique are so costly, therefore, there is need to synthesis ZnO and Mg-ZnO TFs by using simple and cost-effective technique. Here in, we have synthesized ZnO and Mg-ZnO TFs by using a simple and cost-effect material synthesis technique so called evaporation technique.

In this research work, the ZnO and Mg-ZnO TFs are synthesized on glass substrates by evaporation technique in two steps: (i) synthesis of ZnO and (ii) the Mg-ZnO TFs by exposing the synthesized ZnO TFs to evaporated Mg contents for different (30, 60 and 120 second) exposure times. The synthesized ZnO and Mg-ZnO TFs are characterized with X-rays diffraction (XRD), scanning electron microscope (SEM) attached with energy dispersive X-rays spectroscopy (EDX) and UV spectrometer in order to study the crystal structure, surface morphology, elemental compositions, absorption and energy (Eg) band gap.

2. Experimental setup

A simple and cost-effect evaporation technique is employed to synthesize un-doped ZnO and Mg-doped ZnO TFs on glass substrates. Figure 1 demonstrates the schematic diagram of thermal evaporator used to synthesize un-doped ZnO and Mg-doped ZnO TFs. The more detailed information of thermal evaporation technique being used to synthesize various semiconductor materials in the form of layers can be found in literature [19].

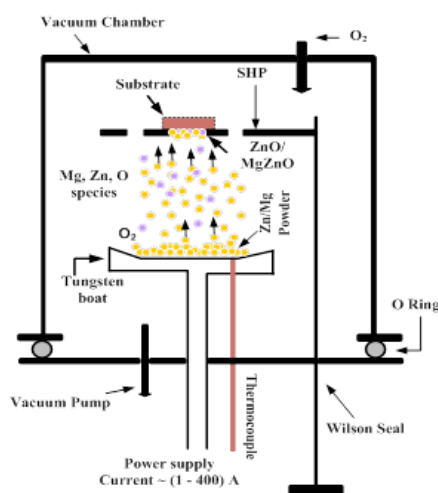
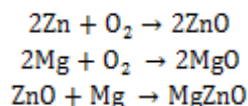


Fig. 1. Schematic diagram of thermal evaporator used to synthesize un-doped ZnO and Mg-doped ZnO TFs.

Prior to synthesis process, the glass substrates are washed with acetone and deionized water. The washed substrate is placed at 3 cm in front of boat connected to digital temperature meter through thermocouple. Thermocouple is used to measure the temperature of boat. The boat temperature is increased by using current power supply. The current of power supply is ranged from 1-400 A. The vacuum chamber is evacuated down to the pressure of 10^{-2} mbar with rotary pump. A shutter is placed between the substrate and boat to avoid from impurities incorporation. The source materials (Zn and Mg) in the form of powders are of analytical grade. The source materials are placed in boat whose temperature is adjusted to 500°C (for Zn) and 800°C (for Mg) by using current power supply. The synthesis parameters of un-doped ZnO TFs on glass substrates are (i) oxygen gas pressure = 1 mbar, (ii) temperature of TB = 500°C , (iii) source to substrate

distance = 3 cm and evaporation time = 120 secs. The basic mechanism behind the synthesis process of un-doped ZnO TFs is: the source material (Zn) placed in boat (500°C) gets enough energy results in their atomic vibrations, bond breaking takes place and hence evaporated in the form of atoms, molecules and ions. The evaporated Zn species, travelling towards substrate surface through oxygen environment (1 mbar), may or may not react with oxygen species depending on their energies. It is known [20] that the evaporated Zn species are of different kinds: (i) some evaporated Zn species are of highly energetic which condense on the substrate surface without making any reaction with oxygen species while (ii) some evaporated Zn species have enough energy and time to react with oxygen species results in the formation of ZnO phase which condense on the substrate surface in the form of layer. A set of four ZnO TFs is synthesized on glass substrates. These synthesized ZnO TFs are called un-doped ZnO TFs. The Mg-doped ZnO TFs are synthesized as: the un-doped ZnO TFs are further exposed to Mg contents for different (30, 60 and 120 secs) times. The other constant synthesis parameters of Mg-doped ZnO TFs are: (i) no working gas, (ii) chamber pressure (10^{-2} mbar). The basic mechanism of Mg evaporation is similar to that of Zn, however, the evaporated Mg species are more energetic comparatively because they travelled through vacuum and could not loss their energy through collisions as well as Mg species are evaporated at higher temperature. These energetic Mg species strike the surface of un-doped ZnO TFs where they may incorporate interstitially in to ZnO lattice or substituted by Zn species. The incorporation of Mg interstitially into ZnO lattice or substituted by Zn is responsible to create lattice distortion, micro-strains and point defects. The probable kinetic equations between involved species (Zn, O and Mg) are demonstrated as:



2. Results and discussions

2.1. XRD analysis

The XRD analysis is used to explore the structural parameters of un-doped ZnO and Mg-doped ZnO TFs synthesized in two steps (already discussed). The average crystallite size (C S), micro-strain (ϵ), dislocation density (δ) and d -spacing are calculated by using the following relations [21-23].

$$\begin{aligned} \text{CS} &= \frac{k\lambda}{\text{FWHM} \cos\theta} \\ \epsilon &= \frac{\text{FWHM} \cos\theta}{4} \\ \delta &= \frac{1}{(\text{CS})^2} \\ 2d \sin\theta &= n\lambda \\ \frac{1}{d_{(hkl)}^2} &= \frac{4}{3} \left(\frac{h^2 + hk + k^2}{a^2} \right) + \frac{1}{c^2} \end{aligned}$$

where $k = 0.9$ (numerical constant), $\lambda = 0.154$ nm (wavelength of incident radiation) and FWHM is the full width at half maximum of the corresponding diffraction peak.

Figure 2 demonstrates the XRD pattern of un-doped ZnO and Mg-doped ZnO TFs synthesized on glass substrates for different (30, 60 and 120 sec) exposure times. The XRD pattern shows the development of ZnO (100), ZnO (002), ZnO (101), ZnO (102), ZnO (110) and ZnO (103) planes appeared at 2θ values of 31.94° , 34.65° , 36.08° , 47.70° , 56.70° and 63.82° respectively [Reference code: 01-075-1526]. This confirms the synthesis of polycrystalline ZnO Phase,

however, it grows preferentially along (002) orientation since its peak intensity is maximum. The intensity of all diffraction planes except (002) plane is increased when the synthesized ZnO TF is exposed to evaporated Mg contents for 30 secs, along with the development of (112) plane appeared at 68.69° . The intensity of all diffraction planes is decreased when the synthesized ZnO TF is further exposed to Mg contents for 60 and 120 secs. It is obvious that the maximum peak intensity is observed at lower exposure (30 secs) time. The increasing and decreasing behavior of peak intensity of ZnO planes is due to doping of Mg contents following by crystallization and recrystallization mechanisms. The development of no diffraction plane related to second phase and the shifting of diffraction planes of ZnO phase indicate the doping of Mg contents into ZnO lattice.

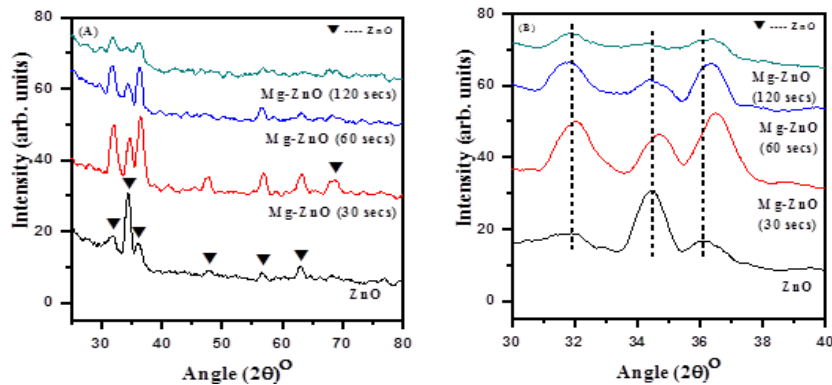


Fig. 2. XRD patterns of (A) un magnified ZnO, Mg-ZnO and (B) magnified Mg-ZnO TFs.

Figure 2_B shows the shifting of diffraction planes of ZnO phase with respect to their stress free values [Reference code: 01-075-1526]. This indicates the presence of residual stresses. It is known that up shifting of diffraction plane indicates the presence of compressive stresses while down shifting of diffraction planes exhibits the existence of tensile stresses [24]. The development of several diffraction planes are related to polycrystalline hexagonal wurtzite structure of ZnO and there is no other secondary phase is detected in the XRD patterns [figure 2_(A, B)]. Putri et al [25] have reported that the shifting of diffraction plane and change in lattice parameters of ZnO films indicates the formation of Mn-doped ZnO films. Ganesh et al [26] have reported that all the samples of un-doped and Mn-doped ZnO have diffraction planes at approximately same 2θ values. All the strong and sharp diffraction planes related to ZnO phase are shifting from their stress free values when exposed into Mg contents for different (30, 60 and 120 secs) times. This indicates the formation of Mg-doped ZnO thin films for all exposure (30, 60 and 120 secs) times in Mg contents. It is interesting to note that the un-doped ZnO thin film has a strong diffraction peak along (002) direction showing that the crystal orientation of un-doped ZnO nano-fibers and rounded nanoparticles is along z axis. On the other hand, the Mg-doped ZnO thin film has a strong diffraction plane along (101) direction which shows that the crystal orientation of Mg-doped ZnO nano-chains of nanoparticles is along x and z axis. Three dominant diffraction planes for Mg-doped ZnO nano-fibers and nano-chains of nanoparticles (100), (002) and (101) indicate that the ZnO nano-fibers and nano-chains of nano-particles are grown in a random alignment.

The values of lattice parameters of Mg-doped ZnO nano-chains of nano-particles (synthesized for 30 secs exposure time in Mg contents) are found to be $a = 3.217$ and $c = 5.171$ nm which are significantly lower than the standard values of lattice parameters, $a = 3.249$ and $c = 5.207$ nm of ZnO respectively. This decrease in lattice parameters is due to smaller ionic radii of Mg^{+2} (0.057 nm) than Zn^{+2} (0.074 nm). It is known that the decreasing or increasing values of lattice parameters is due to doping of elements having smaller or larger ionic radii respectively [25, 26]. Interestingly, the values of lattice parameters of Mg-doped ZnO TFs are slightly increased but not greater than standard values when un-doped ZnO TFs are exposed to 60 and 120 secs in Mg contents. This slightly change in lattice parameters may be due to increasing surface transient temperature during higher exposure time in Mg contents. It is known that the energy delivered by Mg species during bombardment is responsible to increase the surface transient

temperature which is further increased with increasing exposure time. In other words, the increase in surface transient temperature behave like increasing annealing temperature and the increasing annealing temperature is responsible to stress relaxation results in decrease of micro-strains and point defects.

Additionally, the more energetic Mg species are incorporated into ZnO lattice due to smaller ionic radius of Mg results in the shifting of diffraction planes and causes to create defects and stresses. The Mg species can be substituted on Zn places results in the shrinking of lattice parameters due to smaller ionic radius of Mg. Moreover, the incorporation or substitution of Mg species into ZnO lattice is increased with increasing exposure time of Mg contents. Hwang et al [27] have reported that the peak intensity of Mg-doped ZnO TFs strongly depends on increasing annealing temperature. In our case, when the synthesized un-doped ZnO TFs are exposed to evaporated energetic Mg contents, the surface transient temperature of un-doped ZnO TFs is increased. This surface transient temperature of un-doped ZnO TFs is increased more and more with increasing exposure time in Mg contents and may act as annealing temperature provided to un-doped ZnO TFs. This increasing substrate transient temperature may affect the intensity and other structural parameters of Mg-doped ZnO TFs.

Figure 3 demonstrates the variation in peak intensity, FWHM and CS of various diffraction planes as a function of exposure times of un-doped ZnO TFs in evaporated Mg contents. It is obvious that the intensity of (002) plane is decreased while the CS of (002) plane is increased with increasing exposure times. A similar increasing/decreasing trends in the intensity and CS of (100) and (101) planes is observed with increasing exposure times. A decreasing trend of FWHM and micro-strain developed in (002) plane is also observed with increasing exposure times. It is interesting to note that the decreasing trends of FWHM and micro-strains for (002) plane is due to increasing substrate transient temperature during exposure time of un-doped ZnO in Mg contents causes to stress relaxation and hence increases crystallite size of Mg-doped ZnO TFs.

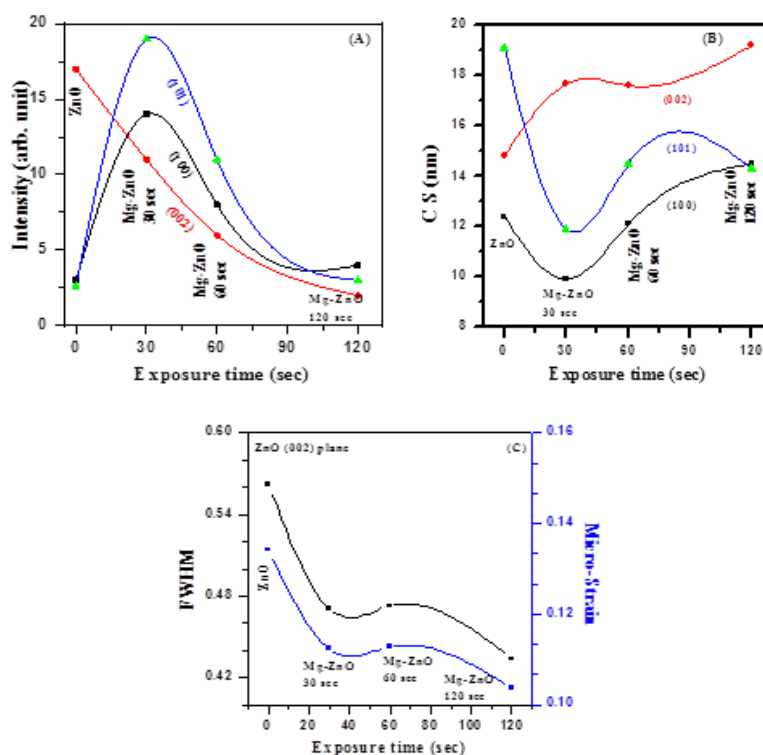


Fig. 3. Variation in (A) peak intensities, (B) C S of (100), (002), (101) plane, (C) FWHM and micro-strains developed in (002) plane of un-doped ZnO and Mg-doped ZnO TFs.

2.2. SEM analysis

The SEM analysis is used to study the surface morphology of synthesized un-doped ZnO and Mg-doped ZnO TFs. Figure 4 exhibits the SEM microstructural features of un-doped ZnO and Mg-doped ZnO TFs. The surface morphology of un-doped ZnO TF indicates the formation of nano-fibers and rounded nanoparticles of sizes ranged from 21-85 nm which are distributed uniformly (figure 4_A). When the un-doped ZnO TF is exposed to Mg contents for 30 secs, the surface morphology of Mg-doped ZnO TF is changed into the formation of nano-chains of rounded nano-particles. The nano-chain of rounded nano-particles is distributed uniformly making the more compact film (figure 4_B). When the un-doped ZnO TF is exposed to Mg contents for 60 secs, the surface morphology of Mg-doped ZnO TF is changed into the formation of nano-chains of rounded nano-particles, however, the size of nano-particles is decreased. The uniform distribution of nano-chains of nano-particles makes more compact Mg-doped ZnO TF (figure 4_C). When the un-doped ZnO TF is exposed to Mg contents for 120 secs, the surface morphology of Mg-doped ZnO TF is again changed into the formation of nano-chains of rounded nano-particles and the formation elongated agglomerates, comprising of smaller size nano-particles. It is obvious that the change in surface morphology, decreasing size of rounded nano-particles, formation of nano-chains and elongated agglomerates and the compactness of Mg-doped ZnO TF are associated with increasing exposure time (figure 4_D). The rise in surface transient temperature of Mg-doped ZnO TFs during the bombardment of evaporated Mg species is responsible to reduce the micro-strains, defects and residual stresses. This statement is agreed well with the XRD analysis.

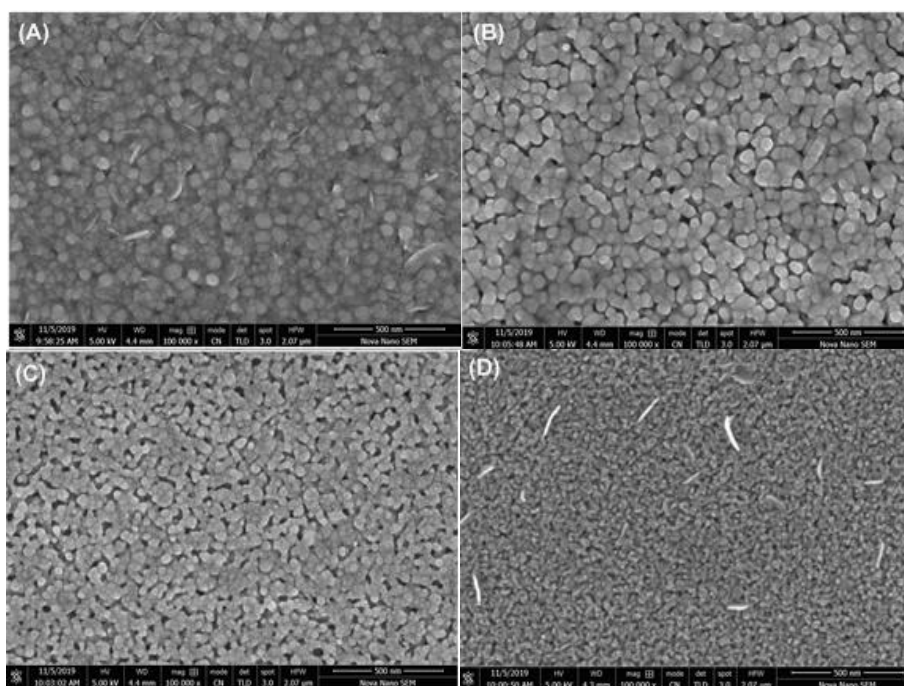


Fig. 4. SEM microstructures of (A) un-doped ZnO and (B), (C), (D) Mg-doped ZnO TFs.

2.3. EDX analysis

The EDX analysis is used to determine the elemental composition of synthesized un-doped ZnO and Mg-doped ZnO TFs. Figure 5 reveals the typical EDX spectrum of Mg-doped ZnO TF synthesized when un-doped ZnO TF is exposed to Mg contents for 120 secs. The development of peaks related to various (Zn, O and Mg) elements confirms the synthesis of Mg-doped ZnO TFs. Table 1 shows the variation of wt.% of Zn, O and Mg with increasing exposure time. Table 1 indicates that the wt.% of Mg is increased with increasing exposure time. The increasing Mg content in Mg-doped ZnO TFs is responsible to increase the film thickness.

Table 1. Wt.% of elements present in un-doped ZnO and Mg-doped ZnO TFs.

Exposure time (sec)	Source material	Working gas	Phases	Elemental composition (Wt. %)		
				Zn	O	Mg
120	Zn	Oxygen	Un-doped ZnO	89.61	8.14	0.57
30	Mg	No working gas	Mg-doped ZnO	88.96	7.91	1.97
60	Mg		Mg-doped ZnO	87.53	7.87	2.93
120	Mg		Mg-doped ZnO	85.52	7.82	4.14

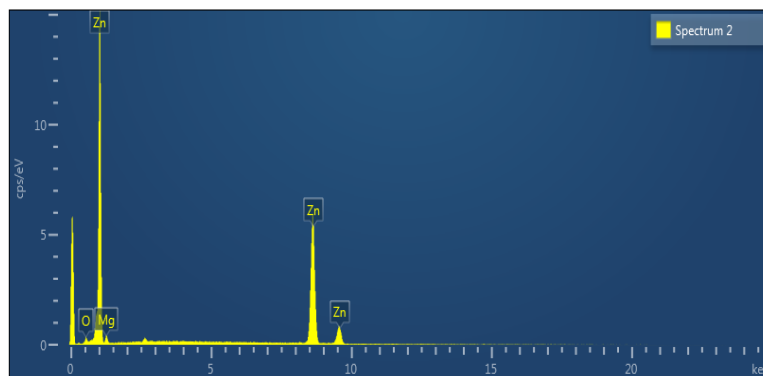


Fig. 5. Typical EDX spectrum of Mg-doped ZnO TF.

2.4. Optical analysis

The optical analysis of un-doped ZnO and Mg-doped ZnO TFs synthesized on glass substrate is performed by employing UV spectrometer. Figure 6 exhibits the change in film thickness, roughness, refractive index and extinction coefficient of un-doped ZnO and Mg-doped ZnO TFs as a function of exposure time of un-doped ZnO TFs in Mg contents. The film thickness and roughness are increased gradually with the increasing exposure time of un-doped ZnO in Mg contents. The increase in film thickness is due to more energy deliverance with increasing exposure time of un-doped ZnO in Mg contents. It means that there is a direct relation between film thickness and roughness whereas there is an inverse relation between film crystallinity (peak intensity; XRD analysis) and film thickness/roughness.

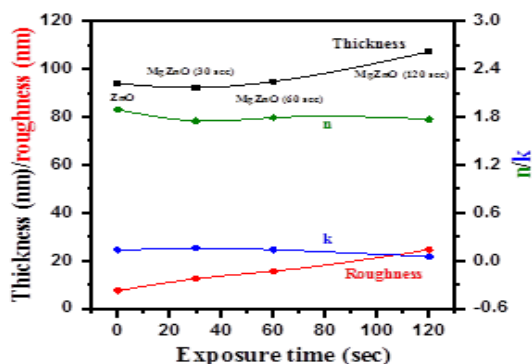


Fig. 6. Variation in film thickness, roughness, refractive index and extinction coefficient as function of exposure time of un-doped ZnO in Mg contents.

The re-crystallization of ZnO phase (XRD analysis) with increasing exposure time in Mg contents is due to lattice distortion causes to generate micro-strains and defects, however, the film

growth rate is increased due to more doping of Mg contents into ZnO lattice. The increasing film thickness and roughness with increasing exposure time in Mg contents is agreed well with the literature [25, 27]. A slight change in refractive index and extinction coefficient of Mg-doped ZnO TFs with increasing exposure time is observed which is due to increase of Mg contents.

The absorption spectra of un-doped ZnO and Mg-doped ZnO TFs are recorded to determine the absorption edge which can be used to measure the E_g of un-doped ZnO and Mg-doped ZnO TFs. Figure 7_A exhibits the absorption spectra of un-doped ZnO and Mg-doped ZnO TFs. The absorption coefficient (α) can be determined from absorption spectra by using the following relation [28].

$$\alpha = \frac{2.303 A}{t}$$

where, A and t stand for absorption and film thickness respectively. The E_g values of un-doped ZnO and Mg-doped ZnO TFs is determined by using the following Tauc's equation [29-31]:

$$\alpha h\nu = A (h\nu - E_g)^m$$

where h is plank's constant, ν is frequency of Photon, A is constant known as characteristic parameter and the value of exponent " m " is equal to $\frac{1}{2}$ for direct band gaps. The ZnO is a semiconducting material which has direct band gap, so we use $m = \frac{1}{2}$ in this case because it provides linear plot between $h\nu$ and $(\alpha h\nu)^2$ [32]. The extrapolating of linear portion of the graph between $h\nu$ and $(\alpha h\nu)^2$ gives the values of E_g of un-doped ZnO and Mg-doped ZnO TFs. It is clear that the absorption edge (Σ 376 nm) of un-doped ZnO TFs is shifted towards lower wavelength with increasing exposure time of ZnO which is due to Burstein-Moss-Effect [33-36]. Figure 7_B exhibits the change in E_g values of Mg-doped ZnO TFs with increasing exposure time. The E_g value of un-doped ZnO (3.05 eV) phase is increased (3.08, 3.19 and 3.29 eV) with increasing doping contents of Mg (increasing exposure time: 30, 60 and 120 sec) into ZnO lattice respectively.

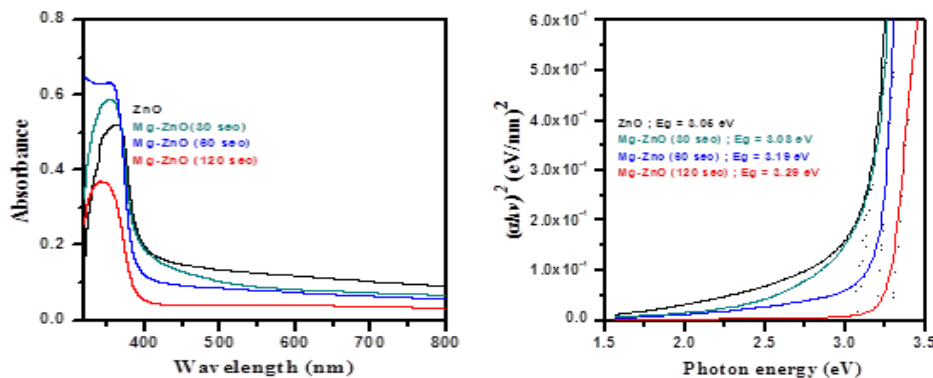


Fig. 7. The change in absorption edge (A) and the E_g values (B) of ZnO and Mg-doped ZnO TFs synthesized for different exposure time of ZnO in Mg contents.

It has been reported that the E_g values of ZnO TFs is increased from 3.02 to 3.74 eV and 3.14 to 3.42 eV by Mg doping [37, 38]. Moreover, similar values of E_g of ZnO and Mg-doped ZnO are found in literature [39-44]. The increase in E_g values of Mg-doped ZnO TFs is due to the creation of lattice distortion, point defects, residual stresses, micro-strains, separation of grains through grain boundaries and compact distribution of agglomerates with increasing exposure time of ZnO in Mg contents. Results show that the synthesized ZnO and Mg-doped ZnO TFs are suitable for optoelectronics and solar cells applications.

3. Conclusion

The un-doped ZnO and Mg-doped ZnO TFs are synthesized on glass substrates by simple and cost-effective evaporation technique. The synthesized un-doped ZnO films are further exposed to evaporated Mg contents for different (30, 60 and 120 sec) times. The XRD patterns reveal the development of ZnO (100), ZnO (002), ZnO (101) diffraction planes thereby confirming the synthesis of ZnO and Mg-doped ZnO polycrystalline films. The values of crystallite size of (100), (101) and (002) planes lies in the range from (12.43-14.51 nm), (14.28-19.08 nm) and (14.78-19.19 nm) respectively with increasing exposure times in Mg contents. The shifting of diffraction plane and shrinking of lattice parameters are due to Mg doping into ZnO lattice. The SEM analysis indicates that the surface morphology of polycrystalline un-doped ZnO Mg-doped ZnO TFs consists of nano-fibers and nano-chains of rounded nanoparticles.

The EDX analysis confirms that the Mg content in ZnO lattice is increased with increasing exposure time. The E_g value of un-doped ZnO (Σ 3.05 eV) is increased to Σ 3.29 eV due to Mg doping. The increase in E_g values of Mg-doped ZnO TFs is due to the creation of lattice distortion, point defects, residual stresses, micro-strains, separation of grains through grain boundaries and compact distribution of agglomerates which are associated with increasing Mg contents. The synthesized ZnO and Mg-doped ZnO TFs are suitable for optoelectronics and solar cells applications.

Acknowledgements

The authors would like to thanks the Higher Education Commission, Pakistan for providing funds to install thermal evaporator at Thin Film Deposition Lab, Department of Physics, Government College University Faisalabad, Pakistan.

References

- [1] P. I Reyes, C-J. Ku, Z. Duan, Y. Lu, A. Solanki, K-B. Lee, *Applied Physics Letters* **98**, 173702 (2011).
- [2] K. Liu, M. Sakurai, M. Aono, *Sensors* **10**, 8604 (2010).
- [3] M. Ahmad, J. Zhu, *Journal of Materials Chemistry* **21**, 599 (2011).
- [4] N. Hirahara, B. Onwona-Agyeman, M. Nakao, *Thin Solid Films* **520**, 2123 (2012).
- [5] N. Yamamoto, H. Makino, Y. Hirashima, *Journal of the Electrochemical Society* **157**, J13 (2010).
- [6] K-K. Kim, S. Niki, J-Y. Oh, *Journal of Applied Physics* **97**, 066103 (2005).
- [7] S. Ozturk, N. Kilinc, N. Tasaltin, Z. Z. Ozturk, *Thin Solid Films* **520**, 932 (2011).
- [8] A. Stadler, *Materials* **5**, 661 (2012).
- [9] A. N. Andriotis, M. Menon, *J Applied Physics* **117**, 125708 (2015).
- [10] V. Etacheri, R. Roshan, V. Kumar, *ACS Appl. Mater. Interfaces* **4**, 2717 (2012).
- [11] Y. Hu, B. Cai, Z. Hu, Y. Liu, S. Zhang, H. Zeng, *Curr. Appl. Physics* **15**, 423 (2015).
- [12] R. Ghosh, D. Basak, *Applied Physics* **101**, 113111 (2007).
- [13] A. Singh, D. Kumar, P. K. Khanna, A. Kumar, M. Kumar, M. Kumar, *Thin Solid Films* **519**, 5826 (2011).
- [14] N. B. Chen, C. H. Sui, *Mater. Sci. Eng. B* **126**, (2006).
- [15] Y. Hu, H. Zeng, J. Du, Z. Hu, S. Zhang, *Mater. Chem. Physics* **182**, 15 (2016).
- [16] A. Kaushal, D. Kaur, *Sol. Energy Mater. Sol. Cells* **93**, 193 (2009).
- [17] J. Sengupta, A. Ahmed, R. Labar, *Mater. Chem. Physics* **109**, 265 (2013).
- [18] D. Fang, C. Li, N. Wang, P. Li, P. Yao, *Cryst. Res. Technol.* **48**, 265 (2013).
- [19] S. A. Hussain, Rehana, B. Hassan, N. Kanwal, S. Pervaiz, M. Razzaq, I. A. Khan, *Journal of Ovonic Research*, **15**, 411 (2019).
- [20] I. A. Khan, N. Amna, N. Kanwal, M. Razzaq, A. Farid, N. Amin, U. Ikhlaq, M. Saleem, R. Ahmad, *Mater. Res. Express* **4**, 036402 (2017).

- [21] X. S. Wang, Z. C. Wu, J. F. Webb, Z. G. Liu, *Appl. Phys. A* **77**, 561 (2003).
- [22] Z. R. Khan, M. S. Khan, M. Zulfequar, M. S. Khan, *Mater. Sci. Appl.* **2**, 340 (2011).
- [23] B. D. Cullity, S. Rstock, *Elements of X-ray Diffraction* Prentice Hall New Jersey (2001).
- [24] I. A. Khan, M. Hassan, R. Ahmad, A. Qayyum, G. Murtaza, M. Zakaullah, R. S. Rawat, *Thin Solid Films* **516**, 8255 (2008).
- [25] N. A. Putri, Y. Febrianti, I. Sugihartono, V. Fauzia, D. Handoko, *AIP Conf. Proc.* 030046-1-030046-4 (1862).
- [26] R. S. Ganesh, E. Durgadevi, M. Navaneethan, V. L. Patil, S. Ponnusamy, C. Muthamizhchelvan, S. Kawasaki, P. S. Patil, Y. Hayakawa, *J. of Alloys and Compounds* **721**, 182 (2017).
- [27] J. D. Hwang, J. S. Lin, S. B. Hwang, *J. Phys. D: Appl. Phys.* **48**, 405103 (2015).
- [28] M. Caglar, Y. Caglar, S. Ilcan, *J. Optoelectron. Adv. Mat.* **8**, 1410 (2006).
- [29] A. Iqbal, A. Mahmood, T. M. Khan, E. Ahmed, *Progress in Natural Science: Materials International* **23**, 64 (2013).
- [30] R.-C. Chang, S.-Y. Chu, P.-W. Yeh, C.-S. Hong, P.-C. Kao, Y.-J. Huang, *Sensors and Actuators B: Chemical* **132**, 290 (2008).
- [31] J. Tauc, R. Grigorovici, A. Vancu. *physica status solidi B* **15**, 627 (1966).
- [32] M. Shakir, S. Kushwaha, K. Maurya, G. Bhagavannarayana, M. Wahab, *Solid State Communications* **149**, 2047 (2009).
- [33] M. Shkir, I. S. Yahia, V. Ganesh, H. Algarni, S. AlFaify, *Materials Letters* **176**, 135 (2016).
- [34] A. Bedia, F. Z. Bedia, M. Aillerie, N. Maloufi, B. Benyoucef, *Energy Procedia* **74**, 529 (2015).
- [35] D. Fang, C. Li, N. Wang, P. Li, P. Yao, *Cryst. Res. Technol.* **48**, 265 (2013).
- [36] K. T. R. Reddy, P. Prathap, N. Revathi, A. S. N. Reddy, R. W. Miles, *Thin Solid Films* **518**, 1275 (2009).
- [37] J. Singh, P. Kumar, K. S. Hui, K. N. Hui, K. Ramam, R. S. Tiwari, *Cryst. Eng. Comm.* **14**, 5898 (2012).
- [38] H. Chen, J. Ding, W. Guo, F. Shi, Y. Li, *Appl. Surf. Science* **258**, 9913 (2012).
- [39] P. Giri, P. Chakrabarti, *Superlattices and Microstructures* **93**, 248 (2016).
- [40] S. Mondal, *International Journal of Advanced Research in Engineering and Technology* **9**, 147 (2018).
- [41] M. Shkir, M. Arif, V. Ganesh, M. A. Manthrammel, A. Singh, I. S. Yahia, S. R. Maidur, P. S. Patil, S. AlFaify, *Journal of Molecular Structure* **1173**, 375 (2018).
- [42] K. Chongsri, W. Techitdheera, W. Pecharapa, *International Journal of Nanotechnology* **11**, 263 (2014).
- [43] N. H. Hashim, S. Subramani, M. Devarajan, A. R. Ibrahim, *Journal of the Australian Ceramic Society* **53**, 421 (2017).
- [44] J. Sengupta, A. Ahmed, R. Labar, *Materials Letters* **109**, 265 (2013).
-